

1 **Strand-specific single-cell methylomics reveals distinct modes of DNA demethylation**
2 **dynamics during early mammalian development**

3
4 Maya Sen^{1†}, Dylan Mooijman^{1,2†}, Jean-Charles Boisset¹, Alex Chialastri^{3,4}, Mina Popovic⁵, Björn
5 Heindryckx⁵, Susana M. Chuva de Sousa Lopes^{5,6}, Siddharth S. Dey^{3,4,7*} & Alexander van
6 Oudenaarden^{1*}

7 ¹ Oncode Institute, Hubrecht Institute-KNAW (Royal Netherlands Academy of Arts and Sciences) and
8 University Medical Center Utrecht, Utrecht, The Netherlands.

9 ² Current address: Developmental Biology Unit, European Molecular Biology Laboratory, Heidelberg,
10 Germany.

11 ³ Department of Chemical Engineering, University of California Santa Barbara, Santa Barbara, CA 93106,
12 USA.

13 ⁴ Center for Bioengineering, University of California Santa Barbara, Santa Barbara, CA 93106, USA.

14 ⁵ Ghent-Fertility and Stem cell Team (G-FaST), Department of Reproductive Medicine, Ghent University
15 Hospital, 9000 Ghent, Belgium.

16 ⁶ Department of Anatomy and Embryology, Leiden University Medical Center, 2333 ZC Leiden, The
17 Netherlands.

18 ⁷ Neuroscience Research Institute, University of California Santa Barbara, Santa Barbara,
19 CA 93106, USA.

20 † These authors contributed equally to this work.

21
22 *Correspondence should be addressed to A.v.O. (a.vanoudenaarden@hubrecht.eu) and S.S.D
23 (sdey@ucsb.edu)

24
25 **Abstract**

26
27 **DNA methylation (5mC) is central to cellular identity and the global erasure of 5mC from**
28 **the parental genomes during preimplantation mammalian development is critical to reset**
29 **the methylome of terminally differentiated gametes to the pluripotent cells in the**
30 **blastocyst. While active and passive modes of demethylation have both been suggested**
31 **to play a role in this process, the relative contribution of these two mechanisms to**
32 **genome-wide 5mC erasure remains unclear. Here, we report a new high-throughput**
33 **single-cell method (scMspJI-seq) that enables strand-specific quantification of 5mC,**
34 **thereby allowing us to systematically probe the dynamics of global demethylation. First,**
35 **when applied to hybrid mouse embryonic stem cells, we identified substantial cell-to-cell**
36 **strand-specific 5mC heterogeneity, with a small group of cells displaying asymmetric**

37 **levels of 5mCpG between the two DNA strands of a chromosome suggesting loss of**
38 **maintenance methylation. Next, using scMspJI-seq in preimplantation mouse embryos,**
39 **we discovered that methylation maintenance is active till the 16-cell stage followed by**
40 **passive demethylation in a fraction of cells within the early blastocyst at the 32-cell stage**
41 **of development. Finally, we found that human preimplantation embryos qualitatively**
42 **show temporally delayed yet similar demethylation dynamics as mouse preimplantation**
43 **embryos. Collectively, these results demonstrate that scMspJI-seq is a sensitive and**
44 **cost-effective method to map the strand-specific genome-wide patterns of 5mC in single**
45 **cells, thereby enabling quantitative investigation of methylation dynamics in**
46 **developmental systems.**

47
48 In mammalian systems, DNA methylation (5-methylcytosine or 5mC) is a key epigenetic
49 modification that is typically stably inherited from mother to daughter cells¹. This property of 5mC
50 plays an important role in facilitating the propagation of cellular identity through cell divisions and
51 restricting the developmental potential of terminally differentiated cells^{1,2}. Consequently, during
52 preimplantation mammalian development, DNA methylation patterns on the terminally
53 differentiated paternal sperm and maternal egg genomes are erased post-fertilization at a
54 genome-wide scale to revert cellular memory towards an undifferentiated state in the blastocyst³.
55 Therefore, understanding the mechanisms underlying global DNA demethylation dynamics is
56 central to understanding the emergence of pluripotent cells during early development.

57 Removal of 5mC can proceed through two alternate mechanisms – passive and active
58 demethylation. Methylated cytosines, within a CpG dinucleotide context are typically copied over
59 to the newly synthesized DNA strands during genome replication by the maintenance
60 methyltransferase, Dnmt1⁴. Passive demethylation relies on loss of 5mC through replicative
61 dilution, in which inhibition of DNA methylation maintenance results in a reduction of 5mC levels
62 after cell division and can be detected through asymmetric levels of 5mC on the two DNA strands
63 of a chromosome. Alternatively, active mechanisms of 5mC erasure occur via conversion of 5mC
64 to 5-hydroxymethylcytosine (5hmC) and other oxidized derivatives, that are not recognized by the
65 DNA maintenance methylation machinery and are subsequently removed by base-excision repair
66 pathways⁵⁻⁷. While early immunofluorescence-based studies revealed that the paternal genome
67 undergoes active demethylation through conversion to 5hmC in the zygote, the maternal genome
68 undergoes passive demethylation through the lack of Dnmt1 activity during replication⁸⁻¹¹.
69 Improving upon this coarse quantification of methylation dynamics, next-generation sequencing
70 and mass spectroscopy based studies have recently revealed that the orthogonal regulation of

71 demethylation by active and passive mechanisms for the two parental genomes is not as distinct
72 as suggested by these early studies¹²⁻¹⁸. However, the conclusions in these recent studies were
73 partly based on bulk bisulfite-sequencing based methods that could not directly distinguish
74 between active vs. passive demethylation, and therefore the relative contribution of these two
75 mechanisms to 5mC reprogramming remains poorly understood.

76 To distinguish between these two mechanisms of demethylation requires strand-specific
77 detection of 5mC in single cells. While asymmetric levels of 5mC between two DNA strands of a
78 chromosome would indicate passive demethylation, the global loss of methylation coupled with
79 symmetric levels of 5mC between two DNA strands would indirectly imply active demethylation
80 (Fig. 1a). Bisulfite-based methods cannot distinguish between 5mC and 5hmC, and importantly
81 when applied to bulk cellular populations, this approach cannot be used to quantify the relative
82 levels of 5mC between two strands of a single chromosome¹⁹. Therefore, to identify the
83 mechanisms regulating DNA demethylation dynamics, we developed a high-throughput method
84 called scMspJI-seq to strand-specifically quantify 5mC on a genome-wide scale in single cells.
85 Single cells are isolated into 384-well plates by fluorescence activated cell sorting or manual
86 pipetting. Following cell lysis and protease treatment to remove chromatin, 5hmC sites in genome
87 DNA (gDNA) are glucosylated using T4 phage β -glucosyltransferase (Fig. 1b). This modification
88 blocks downstream detection of 5hmC and therefore, unlike bisulfite-based methods enables
89 detection of only 5mC. Next, the restriction enzyme MspJI is added to the reaction mixture that
90 recognizes ^mCNNR sites in the genome and creates double-stranded DNA breaks 16 bp
91 downstream of the methylated cytosines leaving a 4-nucleotide 5' overhang²⁰. Thereafter, double-
92 stranded DNA adapters containing a 4-nucleotide 5' overhang are ligated to the fragmented gDNA
93 molecules. These double-stranded DNA adapters, similar in design to those previously developed
94 by us, contain a cell-specific barcode, a random 3 bp unique molecule identifier (UMI) to label
95 individual 5mC sites on different alleles, a 5' Illumina adapter and a T7 promoter^{21,22}. The ligated
96 molecules are then amplified by *in vitro* transcription and used to prepare Illumina libraries as
97 described previously (Fig. 1b)^{21,22}.

98 To validate the method, we first applied scMspJI-seq to single E14TG2a (E14) mouse
99 embryonic stem cells (mES) cells. We found that 97.5% of the 5mCpG sites detected by scMspJI-
100 seq in single cells overlapped with methylated sites observed in bulk bisulfite sequencing of E14
101 gDNA²³. Further, as reported previously, we found that MspJI cuts gDNA 16 bp downstream of
102 the methylated cytosine (Supplementary Fig. 1a)²⁰. Most importantly, due to the maintenance
103 activity of Dnmt1 in E14 cells, we observed similar levels of 5mC on both DNA strands of a
104 chromosome in single cells, as expected (Supplementary Fig. 1b). To quantify the strand-specific

105 distribution of 5mCpG on each chromosome of a single cell, we defined a metric called as strand
106 bias (denoted by f), which is the ratio of the number of 5mCpG sites detected on the plus strand
107 divided by the total number of 5mCpG sites detected on both the plus and minus strands. Finally,
108 to ensure that scMspJI-seq can detect differences in 5mCpG distribution between the two strands,
109 and to confirm that the observed strand bias of 0.5 in E14 cells results from the maintenance
110 activity of Dnmt1, we used CRISPR-Cas9 to knockout *Dnmt1*. We observed a dramatic increase
111 in strand bias in E14 cells without *Dnmt1*, strongly suggesting that our new technology provides
112 a sensitive readout of strand-specific methylation and the ability to distinguish between passive
113 and active demethylation (Supplementary Fig. 1c).

114 During preimplantation development, the maternal and paternal genomes display
115 dramatically different 5mC erasure dynamics, and therefore we next wanted to test our ability to
116 quantify strand-specific 5mC at the resolution of individual alleles. As the single-cell
117 measurements in E14 cells did not provide allele-specific detection of 5mC for each chromosome,
118 we applied scMspJI-seq to hybrid serum grown mES cells (CAST/EiJ x 129/Sv background)²².
119 While the majority of cells displayed methylation maintenance as expected, we surprisingly
120 observed a small population of cells that showed strong 5mC strand bias (Fig. 2). For example,
121 cell 562 displayed similar levels of 5mCpG on the two DNA strands of chromosomes across both
122 alleles (Fig. 2a), whereas cell 216 showed substantially different levels of 5mC on each DNA
123 strand of a chromosome (Fig. 2b). Pearson correlation coefficient (r) between the plus and minus
124 strands of individual cells show that while a majority of cells displayed high correlation, a small
125 subset of cells were weakly correlated, suggesting loss of methylation maintenance in these cells
126 (Fig. 2c). Allele-specific 5mCpG strand bias further revealed the existence of two epigenetically
127 distinct population of mES cells (Fig. 2d). Taken together with the E14 cells, these results highlight
128 that in the absence of allele-specific measurements, strand-specific 5mC quantification is
129 averaged across both alleles, potentially obscuring a detailed view of the methylation status of
130 the genome. Finally, we find that these two distinct 5mC strand bias patterns are also observed
131 at a sub-chromosomal resolution, suggesting this is genome-wide phenomenon that potentially
132 arises from differential methylation maintenance between individual mES cells (Fig. 2e).

133 To validate this cell-to-cell heterogeneity in 5mC strand bias, we reanalyzed data from a
134 recent study that quantified 5mC in single cells using bisulfite sequencing²⁴. While this method is
135 low throughput, single-cell bisulfite sequencing can potentially also be used to infer strand-specific
136 5mC²⁵. In agreement with our findings using scMspJI-seq, reanalysis of the published dataset
137 also revealed hybrid mES cells with similar levels of 5mC on the plus and minus strands, and a
138 small fraction of cells with substantially different levels of 5mC on the two strands of a

139 chromosome (Fig. 3). These results validate our previous observation of two distinct mES cell
140 populations with and without 5mC strand bias (Fig. 2).

141 After establishing this new method, we next used scMspJI-seq to gain a deeper
142 understanding of the 5mC erasure dynamics during preimplantation mouse development as the
143 mechanistic details regulating this genome-wide reprogramming remains unclear from previous
144 work. Early immunofluorescence-based studies showed that 5mC marks on the paternal genome
145 are converted to 5hmC in the zygote⁸⁻¹¹. As 5hmC is not maintained through cell division, and can
146 be further oxidized to be removed by cytidine deaminase and base excision repair pathways, the
147 paternal genome is effectively demethylated from the 1-cell to early blastocyst stage
148 (approximately E3.5 or 32-cell stage) of development⁷. These same studies also reported that the
149 maternal genome retains 5mC in the zygote⁸⁻¹¹. This observation together with reports that Dnmt1
150 is primarily cytoplasmic during these early cell divisions, indirectly suggested that the maternal
151 genome is passively demethylated through a lack of maintenance methylation²⁶⁻²⁹. However, later
152 studies showed the existence of two isoforms of Dnmt1, with the lowly abundant Dnmt1s isoform
153 present in the nucleus of blastomeres³⁰⁻³². Thus, it remains unclear the extent to which the
154 maternal genome is passively demethylated during these early stages. Further, more recently,
155 bulk 5mC and 5hmC sequencing during these early stages have shown that the maternal genome
156 also carries 5hmC marks, suggesting that the maternal genome also undergoes partial active
157 demethylation¹³. As the mechanisms underlying this critical process of 5mC erasure during
158 embryonic development remains unclear, we used strand-specific detection of 5mC in single cells
159 to probe the dynamics of demethylation more closely.

160 We performed scMspJI-seq on hybrid mouse embryos (CAST/EiJ x C57BL/6 background)
161 from the 2- to 32-cell stage of development. In contrast to previous studies that suggested passive
162 demethylation of the maternal genome due to cytoplasmic localization of Dnmt1, experiments in
163 2-cell hybrid mouse embryos surprisingly revealed that 5mCpG on the maternal genome shows
164 a tight strand bias distribution centered around 0.5, implying similar amounts of the mark of both
165 DNA strands and that Dnmt1-mediated methylation maintenance is active at this stage (Fig. 4a
166 and Supplementary Fig. 2a). To ensure that this lack of strand bias in the maternal genome at the
167 2-cell stage is not a technical artifact or a consequence of high *de novo* methylation activity of
168 Dnmt3a/3b, we quantified the levels of 5mCpA, the most abundant non-CpG methylation, in these
169 cells. Non-CpG methylation is not a substrate for Dnmt1 and is deposited on the genome as a
170 result of the activity of the *de novo* methyltransferases, Dnmt3a and Dnmt3b³³⁻³⁵. In the 2-cell
171 embryos, we found that 5mCpA on the maternal genome showed a bimodal pattern of strand bias
172 distribution, suggesting that the lack of strand bias observed for 5mCpG is possibly a result of the

173 maintenance activity of Dnmt1 and not a consequence of high *de novo* methylation rates by
174 Dnmt3a/3b (Fig. 4b and Supplementary Fig. 2b). Further, we have previously shown that bimodal
175 strand bias distributions for 5hmC in 2-cell mouse embryos arises from the slow kinetics of Tet
176 activity and can be used to identify sister cells^{21,36}. This is because 5hmC is not maintained
177 through cell divisions and new DNA strands have lower levels of 5hmC than older strands,
178 resulting in sister cells exhibiting anti-correlated strand bias patterns over all the chromosomes in
179 a cell. Similarly, as 5mCpA is not maintained through cell division, we found that the strong anti-
180 correlation in 5mCpA between chromosomes of single cells can be used to identify sister cells
181 (Supplementary Fig. 2c,d). These results further imply that at the 2-cell stage of development the
182 kinetics of *de novo* methylation by Dnmt3a and Dnmt3b is slow (Fig. 4b). Taken together, these
183 experiments provide preliminary evidence that the similar levels of 5mCpG found on both DNA
184 strands of chromosomes in 2-cell blastomeres is a result of Dnmt1 maintenance activity.

185 Quantifying the dynamics of demethylation beyond the 2-cell stage, we observed for both
186 the maternal and paternal genomes that a majority of chromosomes displayed no significant
187 5mCpG strand bias up to the 16-cell stage (Fig. 4a and Supplementary Fig. 2a). Surprisingly,
188 beyond the 16-cell stage, we observed a widening of the 5mCpG strand bias distribution,
189 suggesting reduced Dnmt1 maintenance activity (Fig. 4a and Supplementary Fig. 2a). These
190 experiments suggest two distinct phases during preimplantation mouse development – an initial
191 period of Dnmt1-mediated maintenance methylation followed by passive demethylation. Finally,
192 we observed that the 5mCpG strand bias distribution at the 32-cell stage is trimodal. Performing
193 *k*-means clustering on the 5mCpG strand bias in these single cells identified two distinct groups
194 of cells as inferred by the mean silhouette scores – a population with no strand bias and another
195 population with a bimodal strand bias distribution (Fig. 4c,d). Further, within the bimodal
196 population, we observed pairs of cells for which all chromosomes were strongly anti-correlated,
197 suggesting that these pairs are sister cells (Fig. 4e and Supplementary Fig. 2e). These
198 observations reveal the existence of significant cell-to-cell heterogeneity in the genome-wide
199 methylome landscapes of cells within the early blastocyst. Taken together, these results suggest
200 maintenance methylation is active till the 16-cell stage and that from the 16- to 32-cell stage, a
201 fraction of cells within the embryo show strong 5mCpG strand bias and undergo passive
202 demethylation.

203 Finally, to conclusively demonstrate that the absence of 5mCpG strand bias up to the 16-
204 cell stage arises from Dnmt1 mediated maintenance methylation, we performed bulk hairpin
205 bisulfite sequencing. A hallmark of Dnmt1 mediated methylation is that both cytosines in a CpG
206 dyad are symmetrically methylated and therefore we performed bulk hairpin bisulfite sequencing

207 that enables interrogation of the methylation status of CpG dyads³⁷. We observed that the fraction
208 of symmetrically methylated CpG dyads in the genome is high up to the 16-cell stage, with a
209 dramatic reduction at the 32-cell stage (that is matched by an increase in hemi-methylated CpG
210 dyads at this stage), thereby demonstrating that maintenance methylation is active initially and is
211 followed by passive demethylation at the 32-cell stage (Fig. 4f).

212 We finally extended scMspJI-seq to explore the dynamics of global demethylation in
213 human preimplantation embryos, ranging from developmental day 2 to 7. Studies in human
214 preimplantation embryos have shown temporally slower, yet similar developmental dynamics to
215 mouse embryos³⁸. Despite lacking allelic information, our results suggest that the mouse and
216 human 5mCpG demethylation dynamics are similar, with an initial phase till the 16-cell stage
217 displaying a tight 5mCpG strand bias distribution centered around 0.5, followed by an increase in
218 strand bias in a small fraction of cells from the 32- to 128-cell stage (Fig. 5a and Supplementary
219 Fig. 3a). This is consistent with previous immunostainings in human preimplantation embryos that
220 show a decrease in DNMT1 protein levels between Day 5 and Day 6 blastocysts^{39,40}. Further,
221 5mCpA strand-bias distributions of human preimplantation embryos appear to be similar to the
222 trend observed in mouse embryos with a majority of cells till the 16-cell stage displaying 5mCpA
223 strand bias (Fig. 5b and Supplementary Fig. 3b). Finally, upon closer inspection of 5mCpA strand
224 bias per cell, we observed three sister pairs in Day 3 embryos with a mirrored pattern of strand
225 bias along the entire genome (Supplementary Fig. 3c).

226 In summary, we have developed a new high-throughput strand-specific method that
227 enables us to quantify 5mC on a genome-wide scale in single cells. When applied to serum grown
228 mES cells, we found substantial cell-to-cell variability in strand-specific 5mC landscapes,
229 revealing the existence of chromosome-wide heterogeneity in the methylome of mES cells.
230 Reanalysis of a previous single-cell bisulfite sequencing study further confirmed these results²⁴.
231 Furthermore, in addition to exploring strand-specific 5mC heterogeneity in single cells, scMspJI-
232 seq also enables systematic investigation of the mechanisms regulating demethylation dynamics.
233 In preimplantation mouse embryos, we surprisingly discovered two distinct phases of methylation
234 dynamics – an initial phase till the 16-cell stage where methylation maintenance is active, followed
235 by loss of maintenance in a fraction of cells within the early blastocyst at the 32-cell stage. These
236 results further highlight the presence of strand-specific 5mC heterogeneity between individual
237 cells during early mammalian development. In future, we plan to explore how this genome-wide
238 heterogeneity in the methylome regulates lineage commitment during development. Finally,
239 despite the reduced resolution due to lack of allelic information, we found similar demethylation
240 dynamics in preimplantation human embryos. Thus, scMspJI-seq presents a new single-cell

241 strand-specific technology that potentially can be used to probe the dynamics of methylation
242 during development, cancer progression, aging and in other biological systems.

243 **METHODS**

244

245 **Cell culture**

246 E14tg2a mouse embryonic stem cells were obtained from American Type Culture Collection
247 (ATCC CRL-182) and the hybrid 129/Sv:CAST/EiJ mouse embryonic stem cells were obtained
248 from Jop Kind's group (Hubrecht Institute). Both lines were tested for mycoplasma contamination.
249 Cells were grown on 0.1% gelatin in ES cell culture media; DMEM (1x) high glucose + glutamax
250 (Gibco), supplemented with 10% FCS (Greiner) 100 μ M β -mercaptoethanol (Sigma), 100 μ M
251 Non-essential amino acids (Gibco), 50 μ g/mL Pen/Strep (Gibco) and 1000 U/mL ESGRO mLIF
252 (Millipore). Cells were split every 2 days and media changed every day. Cells were harvested
253 before FACS by washing 3 times with 1x PBS with calcium and magnesium and incubated with
254 0.05% Trypsin (Life Technologies). Cell were resuspended in ES culture media and cell clumps
255 were removed by passing the cells through a BD Falcon 5 mL polystyrene tube with a filter top.

256

257 **Crispr-Cas9 Dnmt1 knockout**

258 Six gRNA sequences targeting three exons of mouse Dnmt1 were used as described previously⁴¹.
259 Phosphorylated BbsI compatible restriction overhangs were added to gRNA top and bottom oligos
260 and resuspended at 100 μ M in nuclease-free water. Annealing of the oligos was performed in 1x
261 ligation buffer (NEB) using the following program: 97°C for 5 minutes, ramp down by 1°C per 1
262 minute to 20°C. The pX330 CRISPR-Cas9-GFP gRNA plasmid was a kind gift from Eva van Rooij
263 and mixed with 0.1 μ M gRNA oligo. The reaction was simultaneously digested with BbsI (NEB)
264 and ligated with T4 DNA ligase (NEB) overnight at 16°C. Ligation reactions were transformed into
265 DH5 α competent cells and subsequently sequenced using Sanger dideoxy sequencing to confirm
266 the correct insert. All six pX300-gRNA plasmids were pooled and 1 μ g was transfected into 2
267 million E14tg2a cells using Lipofectamine (Life Technologies). A separate pX300 empty vector
268 was also transfected into E14tg2a to serve as a negative control. Two days later, single GFP
269 positive cells were sorted into 384-well plates (BioRad) and subjected to scMspJI-seq.

270

271 **Preimplantation mouse embryo isolation**

272 CAST/EiJ x C57BL/6 hybrid mouse embryos were obtained from four 3-month-old superovulated
273 B6 mothers (injected with pregnant mare serum gonadotropin (PMSG) and human chorionic
274 gonadotropin (HCG) 22 h later) and incubated in M16 medium at 37°C and 5% CO₂. Cells were
275 isolated using hyaluronic acid (Sigma) and trypsin (Life Technologies) and manually deposited
276 into 384-well plates containing lysis buffer and Vapor-lock. Plates were subsequently centrifuged

277 at 1,000 rpm for 1 minute to ensure that cells reach the aqueous phase and then subjected to
278 scMspJI-seq. All animal experiments were approved by the Royal Netherlands Academy of Arts
279 and Sciences and were performed according to the animal experimentation guidelines of the
280 KNAW.

281

282 **Preimplantation human embryo isolation**

283 Supernumerary cryopreserved human embryos were obtained for research from patients
284 undergoing *in vitro* fertilization (IVF) using standard clinical protocols, at the Department for
285 Reproductive Medicine, Ghent University Hospital. Cleavage stage embryos, cryopreserved on
286 day 2 or 3 of development, were warmed using EmbryoThaw™ media (Fertipro, Belgium), as
287 outlined by the manufacturer. Blastocyst stage embryos, vitrified on day 5 or 6 of development,
288 were warmed using the Vitrification Thaw kit (Irvine Scientific, Netherlands), as described⁴².
289 Embryos were transferred to either Cook Cleavage or Cook Blastocyst Medium (COOK, Ireland)
290 depending on their developmental stage, and cultured in 20 µL medium droplets under mineral
291 oil (Irvine Scientific, Netherlands) at 37 °C, 6% CO₂ and 5% O₂. When required, embryos were
292 briefly treated with Acidic Tyrode's Solution (Sigma-Aldrich, Belgium) for removal of the zona
293 pellucida. All embryos were washed and subsequently dissociated by gentle mechanical
294 dissociation in TrypLE Express Enzyme (Life Technologies, Belgium) using glass capillaries.
295 Single blastomeres were washed and manually deposited into 384-well plates containing lysis
296 buffer and Vapor-Lock. Plates were subsequently centrifuged at 1,000 rpm for 1 minute and
297 stored at -80 °C until further processing. This study was approved by the Ghent University
298 Institutional Review Board (EC2015/1114) and the Belgian Federal Commission for medical and
299 scientific research on embryos *in vitro* (ADV_060_UZGent). All embryos were donated following
300 patients' written informed consent.

301

302 **scMspJI-seq**

303 Prior to FACS or manual isolation of single cells, 384-well plates (BioRad) are prepared as follows:
304 4 µL of Vapor-Lock (Qiagen) is manually added to each well using a multichannel pipette followed
305 by 2 µL of lysis buffer (0.2 µL of 25 µg/µL Qiagen Protease, 0.2 µL of 10x NEB Buffer 4 and 1.6
306 µL of nuclease-free water) using the Nanodrop II liquid-handling robot (BioNex Solutions). All
307 downstream dispensing steps are performed using the liquid-handling robot. After spinning down
308 the 384-well plates, single cells are deposited into each well of the plate and incubated at 50°C
309 for 15 hours, 75°C for 20 minutes and 80°C for 5 minutes. 5hmC sites in the genome are then
310 glucosylated to block downstream recognition by MspJI by dispensing 0.5 µL of the following

311 reaction mixture: 0.1 μ L of T4-BGT (NEB), 0.1 μ L of UDP-Glucose (NEB), 0.05 μ L of 10x NEB
312 Buffer 4 and 0.25 μ L of nuclease-free water. After incubation at 37°C for 16 hours, 0.5 μ L the
313 following reaction mixture is added: 0.1 μ L of 25 μ g/ μ L Qiagen Protease, 0.05 μ L of 10x NEB
314 Buffer 4 and 0.35 μ L of nuclease-free water. The plate is then incubated at 50°C for 5 hours, 75°C
315 for 20 minutes and 80°C for 5 minutes. Thereafter, gDNA is digested by the restriction enzyme
316 MspJI by the addition of 0.5 μ L of the following reaction mixture: 0.02 μ L of MspJI (NEB), 0.12 μ L
317 of 30x enzyme activator solution (NEB), 0.05 μ L of 10x NEB Buffer 4 and 0.31 μ L of nuclease-
318 free water. The digestion is performed at 37°C for 5 hours followed by heat inactivation of MspJI
319 at 65°C for 20 minutes. Next, 0.2 μ L of cell-specific double-stranded adaptors are added to
320 individual wells and these adapters are ligated to the fragmented gDNA molecules by adding 0.8
321 μ L of the following reaction mixture: 0.07 μ L of T4 DNA ligase (NEB), 0.1 μ L of T4 DNA ligase
322 buffer (NEB), 0.3 μ L of 10 mM ATP (NEB) and 0.33 μ L of nuclease-free water. The ligation is
323 performed at 16°C for 16 hours. Next, wells containing unique cell-specific adapters are pooled
324 using a multichannel pipette and incubated with 0.8x Agencourt Ampure (Beckman Coulter)
325 beads for 30 minutes, washed twice with 80% ethanol and resuspended in 6.4 μ L of nuclease-
326 free water. Thereafter, *in vitro* transcription and Illumina library preparation is performed as
327 described previously in the scAba-seq protocol.

328

329 **scMspJI-seq adapters**

330 The double-stranded scMspJI-seq adapters are designed to contain a T7 promoter, 5' Illumina
331 adapter, 3 bp UMI, 8 bp cell-specific barcode, and a random 4-nucleotide 5' overhang. The
332 general design of the top and bottom strand is shown below:

333

334 Top oligo:

335 5' –CGATTGAGCCGGTAATACGACTCACTATAGGGGTTCTACAGTCCGACGATCNNN[8 bp cell-barcode] – 3'

336

337 Bottom oligo:

338 5' – NNNN[8 bp cell-barcode]NNNGATCGTCGGACTGTAGAACTCTGAACCCCTATAGTGAGTCGTATTACCGGCCTCAATCG – 3'

339

340 The sequence of the 8 bp cell-specific barcode is provided in Supplementary Table 1. The protocol
341 for phosphorylating the bottom strand and for annealing the top and bottom strands to generate
342 the double-stranded adapters is described previously in the scAba-seq protocol.

343

344

345 **scMspJI-seq analysis pipeline**

346 scMspJI-seq libraries were sequenced on an Illumina NextSeq 500 platform. Reads containing
347 the correct cell-specific barcode were mapped to the mouse (mm10) or human (hg19) genome
348 using the Burrows-Wheeler Aligner (BWA) and filtered for uniquely mapping reads to the genome.
349 Custom scripts written in Perl were then used to demultiplex the data, identify 5mC position, strand
350 information, and remove PCR duplicates. Custom codes will be made available upon request.

351

352 **Strand-specific scNMT-seq analysis pipeline**

353 Bisulfite sequencing data from published scNMT libraries (GSE109262)²⁴ were processed as
354 described previously⁴³. The first nine bases of the raw reads were trimmed using Trim Galore
355 (v0.5.0) and mapped using Bismark (v20) to the mouse genome (mm10) with the 129/CAST
356 background. SNPs specific to 129/CAST mouse genome were prepared using SNPsplit (v0.3.2)
357 and a list of known variant call files from the Mouse Genomes Project
358 (<http://www.sanger.ac.uk/resources/mouse/genomes/>). After mapping with Bismark, duplicate
359 sequences were removed and CpG methylation calls were extracted with strand-specific
360 information. Further data analysis and visualization of the methylation calls used custom scripts
361 that will be made available upon request.

362

363 **Hairpin Bisulfite Sequencing**

364 Hairpin bisulfite sequencing was performed on bulk mouse embryos samples (2- to 64-cell stage
365 mouse embryos). The embryos were treated with protease (1 μ L of 25 μ g/ μ L Qiagen Protease, 1
366 μ L of 10x NEB Buffer 4, and 8 μ L of nuclease-free water). Then, 0.5 ng of genomic DNA was
367 digested with 20 μ L of MspI master mix (1 μ L of MspI (NEB), 2 μ L 10x NEB CutSmart Buffer in a
368 total volume of 20 μ L) and incubated at 37°C for 1 hour. After digestion, the fragmented genomic
369 DNA was ligated with 1 μ L of 10 μ M phosphorylated hairpin oligo mix (1 μ L of NEB T4 ligase, 1
370 μ L of 10x NEB T4 Ligase buffer, 2 μ L of 10mM ATP, 5 μ L of nuclease-free water) and incubated
371 overnight at 16°C. The hairpin oligo was prepared as follows: The oligo (G/iMe-dC/iMe-dC/G/iMe-
372 dC/iMe-dC/GG/iMe-dC/GG/iMe-dC/AAG/iBiodT/GAAG/iMe-dC/iMe-dC/G/iMe-dC/iMe-
373 dC/GG/iMe-dC/G) was resuspended in 100 μ M of Low-TE. The hairpin oligo was then
374 phosphorylated (1 μ L of 100 μ M hairpin oligo, 3 μ L of 10x T4 Ligase Buffer, 1 μ L T4 PNK and 5
375 μ L of nuclease free water) and incubated at 37°C for an hour. Subsequently, the phosphorylated
376 oligo was heated at 94°C and placed in ice water to generate the loop. For purification of the
377 ligation mixture, Dynabeads™ M-280 Streptavidin beads were used following the recommended

378 manufacturer's protocol with the following changes: the bead-ligation mixture was incubated for
379 1 hour at RT on a rotator and a cold 10 mM Tris-HCl wash step was included. Subsequently, we
380 performed bisulfite sequencing on the sample using the protocol described previously⁴⁴. After
381 sequencing the libraries on a Miseq 300 bp or NextSeq 500 75 bp pair-end run, we used HBS-
382 tools and custom Perl scripts to analyze the methylated CpG dyads⁴⁵.

383

384 **Data Availability**

385 Accession code GEO: In preparation

386

387 **Code Availability**

388 Custom codes to detect strand-specific 5mC using scMspJI-seq will be made available upon
389 request.

390 **References**

- 391 1. Cedar, H. & Bergman, Y. Programming of DNA Methylation Patterns. *Annu. Rev. Biochem.*
392 **81**, 97–117 (2012).
- 393 2. Dirk, S. Function and information content of DNA methylation. *Nature* **517**, 321–326 (2015).
- 394 3. Hackett, J. A. & Surani, M. A. DNA methylation dynamics during the mammalian life cycle.
395 *Philos. Trans. R. Soc. Lond., B, Biol. Sci.* **368**, 20110328 (2013).
- 396 4. Leonhardt, H., Page, A. W., Weier, H.-U. & Bestor, T. H. A targeting sequence directs DNA
397 methyltransferase to sites of DNA replication in mammalian nuclei. *Cell* **71**, 865–873 (1992).
- 398 5. Tahiliani, M. *et al.* Conversion of 5-Methylcytosine to 5-Hydroxymethylcytosine in Mammalian
399 DNA by MLL Partner TET1. *Science* **324**, 930–935 (2009).
- 400 6. Ito, S. *et al.* Tet proteins can convert 5-methylcytosine to 5-formylcytosine and 5-
401 carboxylcytosine. *Science* **333**, 1300–1303 (2011).
- 402 7. Wu, X. & Zhang, Y. TET-mediated active DNA demethylation: mechanism, function and
403 beyond. *Nat. Rev. Genet.* **18**, 517–534 (2017).
- 404 8. Wossidlo, M. *et al.* 5-Hydroxymethylcytosine in the mammalian zygote is linked with
405 epigenetic reprogramming. *Nat. Commun.* **2**, 241 (2011).
- 406 9. Mayer, W., Niveleau, A., Walter, J., Fundele, R. & Haaf, T. Demethylation of the zygotic
407 paternal genome. *Nature* **403**, 501–502 (2000).
- 408 10. Inoue, A. & Zhang, Y. Replication-dependent loss of 5-hydroxymethylcytosine in mouse
409 preimplantation embryos. *Science* **334**, 194–194 (2011).
- 410 11. Iqbal, K., Jin, S.-G., Pfeifer, G. P. & Szabo, P. E. Reprogramming of the paternal genome
411 upon fertilization involves genome-wide oxidation of 5-methylcytosine. *Proc. Natl. Acad. Sci.*
412 *U.S.A.* **108**, 3642–3647 (2011).
- 413 12. Smith, Z. D. *et al.* A unique regulatory phase of DNA methylation in the early mammalian
414 embryo. *Nature* **484**, 339–344 (2012).
- 415 13. Wang, L. *et al.* Programming and Inheritance of Parental DNA Methylomes in Mammals. *Cell*
416 **157**, 979–991 (2014).
- 417 14. Arand, J. *et al.* Selective impairment of methylation maintenance is the major cause of DNA
418 methylation reprogramming in the early embryo. *Epigenetics Chromatin* **8**, 1 (2015).
- 419 15. Okamoto, Y. *et al.* DNA methylation dynamics in mouse preimplantation embryos revealed by
420 mass spectrometry. *Sci. Rep.* **6**, 19134 (2016).
- 421 16. Guo, H. The DNA methylation landscape of human early embryos. *Nature* **511**, 606–610
422 (2014).

- 423 17. Smith, Z. D. *et al.* DNA methylation dynamics of the human preimplantation embryo. *Nature*
424 **511**, 611–615 (2014).
- 425 18. Okae, H. *et al.* Genome-Wide Analysis of DNA Methylation Dynamics during Early Human
426 Development. *PLoS Genet.* **10**, e1004868 (2014).
- 427 19. Huang, Y. *et al.* The Behaviour of 5-Hydroxymethylcytosine in Bisulfite Sequencing. *PLoS*
428 *One* **5**, e8888 (2010).
- 429 20. Cohen-Karni, D. *et al.* The MspJI family of modification-dependent restriction endonucleases
430 for epigenetic studies. *Proc. Natl. Acad. Sci. U.S.A.* **108**, 11040–11045 (2011).
- 431 21. Mooijman, D., Dey, S. S., Boisset, J. C., Crosetto, N. & van Oudenaarden, A. Single-cell 5hmC
432 sequencing reveals chromosome-wide cell-to-cell variability and enables lineage
433 reconstruction. *Nat. Biotechnol.* **34**, 852–856 (2016).
- 434 22. Rooijers, K. *et al.* Simultaneous quantification of protein-DNA contacts and transcriptomes in
435 single cells. *Nat. Biotechnol.* **37**, 766–772 (2019).
- 436 23. Habibi, E. *et al.* Whole-Genome Bisulfite Sequencing of Two Distinct Interconvertible DNA
437 Methylomes of Mouse Embryonic Stem Cells. *Cell Stem cell* **13**, 360–369 (2013).
- 438 24. Clark, S. J. *et al.* scNMT-seq enables joint profiling of chromatin accessibility DNA methylation
439 and transcription in single cells. *Nat. Commun.* **9**, 781 (2018).
- 440 25. Lister, R. *et al.* Human DNA methylomes at base resolution show widespread epigenomic
441 differences. *Nature* **462**, 315–322 (2009).
- 442 26. Carlson, L. L., Page, A. W. & Bestor, T. H. Properties and localization of DNA
443 methyltransferase in preimplantation mouse embryos: implications for genomic imprinting.
444 *Genes Dev.* **6**, 2536–2541 (1992).
- 445 27. Cardoso, M. C. & Leonhardt, H. DNA Methyltransferase Is Actively Retained in the Cytoplasm
446 during Early Development. *J. Cell Biol.* **147**, 25–32 (1999).
- 447 28. Howell, C. Y. *et al.* Genomic Imprinting Disrupted by a Maternal Effect Mutation in the Dnmt1
448 Gene. *Cell* **104**, 829–838 (2001).
- 449 29. Ratnam, S. *et al.* Dynamics of Dnmt1 Methyltransferase Expression and Intracellular
450 Localization during Oogenesis and Preimplantation Development. *Dev. Biol.* **245**, 304–314
451 (2002).
- 452 30. Cirio, M. C. *et al.* Preimplantation expression of the somatic form of Dnmt1 suggests a role in
453 the inheritance of genomic imprints. *BMC Dev. Biol.* **8**, 9 (2008).
- 454 31. Kurihara, Y. *et al.* Maintenance of genomic methylation patterns during preimplantation
455 development requires the somatic form of DNA methyltransferase 1. *Dev. Biol.* **313**, 335–346
456 (2008).

- 457 32. Hirasawa, R. *et al.* Maternal and zygotic Dnmt1 are necessary and sufficient for the
458 maintenance of DNA methylation imprints during preimplantation development. *Genes Dev.*
459 **22**, 1607–1616 (2008).
- 460 33. Ramsahoye, B. H. *et al.* Non-CpG methylation is prevalent in embryonic stem cells and may
461 be mediated by DNA methyltransferase 3a. *Proc. Natl. Acad. Sci. U.S.A.* **97**, 5237–5242
462 (2000).
- 463 34. Ziller, M. J. *et al.* Genomic Distribution and Inter-Sample Variation of Non-CpG Methylation
464 across Human Cell Types. *PLoS Genet.* **7**, e1002389 (2011).
- 465 35. Arand, J. *et al.* In vivo control of CpG and non-CpG DNA methylation by DNA
466 methyltransferases. *PLoS Genet.* **8**, e1002750 (2012).
- 467 36. Wangsanuwat, C., Aldeguer, J. F., Rivron, N. C. & Dey, S. S. A probabilistic framework for
468 cellular lineage reconstruction using single-cell 5-hydroxymethylcytosine sequencing. *bioRxiv*
469 doi:<https://doi.org/10.1101/739300>
- 470 37. Zhao, L. *et al.* The dynamics of DNA methylation fidelity during mouse embryonic stem cell
471 self-renewal and differentiation. *Genome Res.* **24**, 1296–1307 (2014).
- 472 38. Iurlaro, M., Meyenn, von, F. & Reik, W. DNA methylation homeostasis in human and mouse
473 development. *Curr. Opin. Genet. Dev.* **43**, 101–109 (2017).
- 474 39. Petrusa, L., Van de Velde, H. & De Rycke, M. Dynamic regulation of DNA methyltransferases
475 in human oocytes and preimplantation embryos after assisted reproductive technologies. *Mol.*
476 *Hum. Reprod.* **20**, 861–874 (2014).
- 477 40. Petrusa, L., Van de Velde, H. & De Rycke, M. Similar kinetics for 5-methylcytosine and 5-
478 hydroxymethylcytosine during human preimplantation development in vitro. *Mol. Reprod. Dev.*
479 **83**, 594–605 (2016).
- 480 41. Sanjana, N. E., Shalem, O. & Zhang, F. Improved vectors and genome-wide libraries for
481 CRISPR screening. *Nat. Methods* **11**, 783–784 (2014).
- 482 42. Van Landuyt, L. *et al.* Closed blastocyst vitrification of biopsied embryos: evaluation of 100
483 consecutive warming cycles. *Hum. Reprod.* **26**, 316–322 (2011).
- 484 43. Smallwood, S. A. *et al.* Single-cell genome-wide bisulfite sequencing for assessing epigenetic
485 heterogeneity. *Nat. Methods* **11**, 817–820 (2014).
- 486 44. Clark, S. J. *et al.* Genome-wide base-resolution mapping of DNA methylation in single cells
487 using single-cell bisulfite sequencing (scBS-seq). *Nat. Protoc.* **12**, 534–547 (2017).
- 488 45. Sun, M.-A., Velmurugan, K. R., Keimig, D. & Xie, H. HBS-Tools for Hairpin Bisulfite
489 Sequencing Data Processing and Analysis. *Adv. Bioinformatics* **2015**, 760423 (2015).
- 490

491 **Acknowledgements**

492 We would like to thank members of the van Oudenaarden and Dey groups for constructive
493 feedback. We thank patients of the Department for Reproductive Medicine, Ghent University
494 Hospital, for donating their cryopreserved embryos for this study. We acknowledge support for
495 the computational work from the Center for Scientific Computing at the California NanoSystems
496 Institute (CNSI) and Materials Research Laboratory (MRL) at UCSB: an NSF MRSEC (DMR-
497 1720256) and NSF CNS-1725797. We thank Ferring Pharmaceuticals (Aalst, Belgium) for an
498 unrestricted educational grant. This work was supported by a Fonds Wetenschappelijk Onderzoek
499 – Vlaanderen (FWO, Research Foundation – Flanders; G051516N) grant to B.H, the De Snoo-
500 van't Hoogerhuijs Stichting to S.C.d.S.L., an European Research Council Advanced grant (ERC-
501 AdG 742225-IntScOmics) and a Nederlandse Organisatie voor Wetenschappelijk Onderzoek
502 (NWO) TOP award (NWO-CW 714.016.001) to A.v.O., and an UC Cancer Research Coordinating
503 Committee (CTN-19-585462) grant and an NIH R01HD099517 grant to S.S.D. This work is part
504 of the OncoCode Institute which is partly financed by the Dutch Cancer Society.

505

506 **Author Contributions**

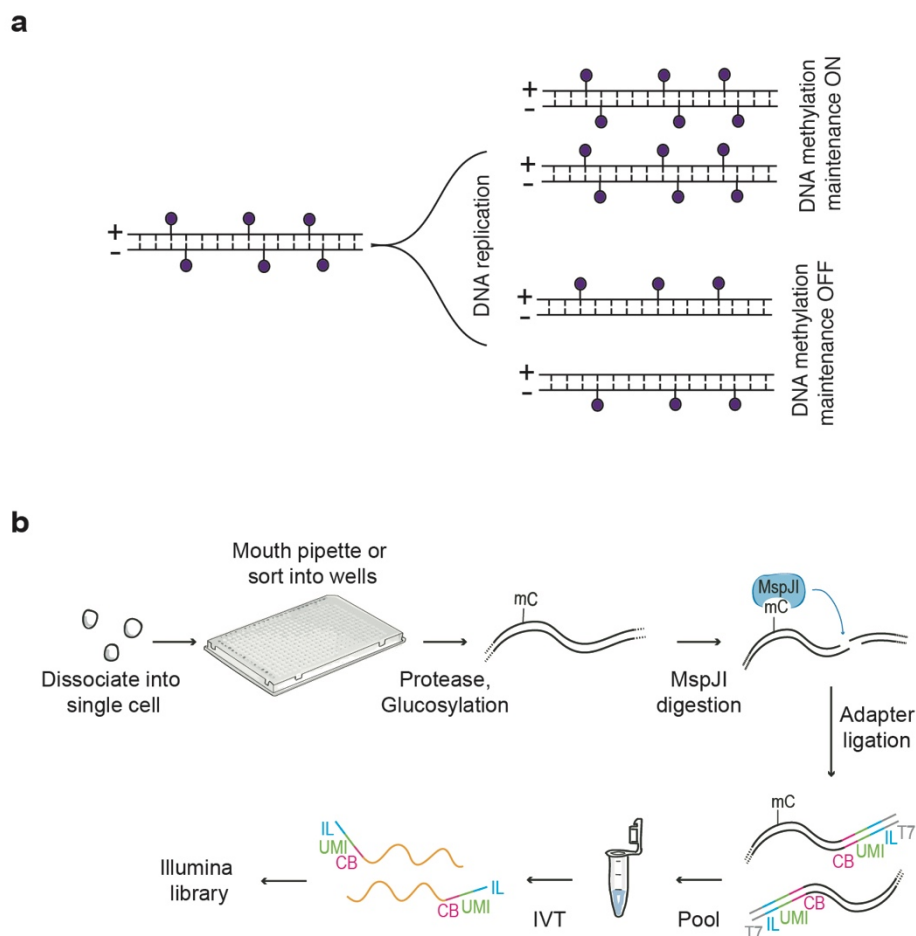
507 M.S., D.M., S.S.D. and A.v.O. designed the study. S.S.D. and D.M. developed the method.
508 S.S.D., M.S., D.M. performed experiments. J.-C.B. and D.M. isolated preimplantation mouse
509 embryos. M.P., S.C.d.S.L. isolated preimplantation human embryos. M.S., D.M., J.-C.B., A.C.,
510 S.S.D. and A.v.O. analyzed the data. S.S.D., M.S., D.M. and A.v.O. wrote the manuscript.

511

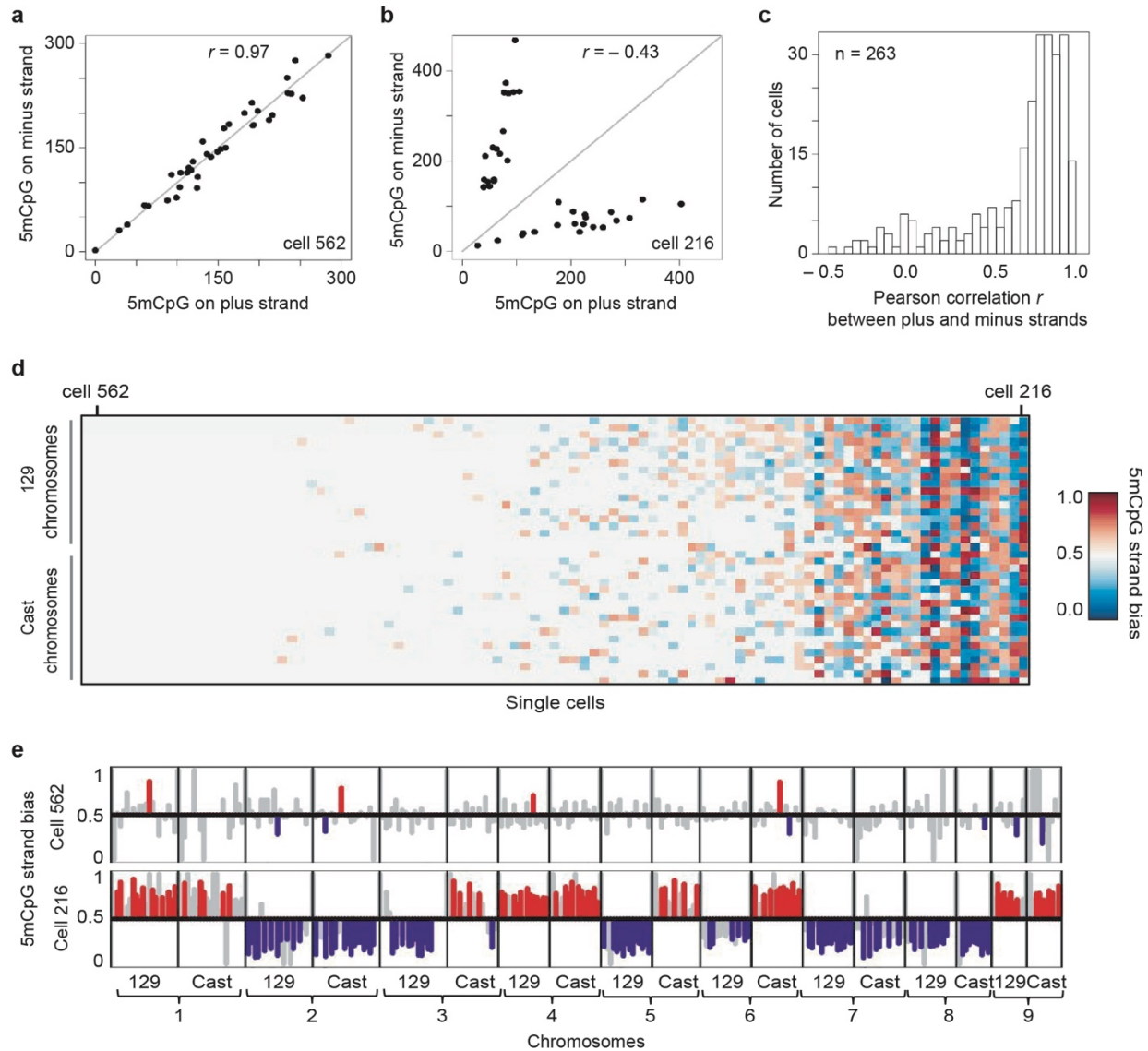
512 **Competing Interests**

513 The authors declare no competing financial interests.

514 **Figures**



515
516 **Figure 1 | Schematic of scMspJI-seq.** (a) DNA methylation maintenance can be probed using
517 strand-specific quantification of 5mC in single cells. Cells displaying methylation maintenance
518 have symmetric levels of 5mCpG on both DNA strands of a chromosome while loss of methylation
519 maintenance results in asymmetric levels of 5mCpG between the two DNA strands. (b) Single
520 cells isolated by FACS or manual pipetting are deposited into 384-well plates and lysed. Following
521 protease treatment to strip off chromatin and blocking of 5hmC sites by glucosylation, MspJI is
522 used to recognize 5mC sites and cut gDNA 16 bp downstream of the methylated cytosine. After
523 ligating double-stranded adapters – containing a cell-specific barcode (CB, pink), a random 3 bp
524 unique molecule identifier to label individual 5mC sites on different alleles (UMI, green), 5' Illumina
525 adapter (IL, blue) and T7 promoter (T7, gray) – to the fragmented gDNA, molecules from all single
526 cells are pooled and amplified by *in vitro* transcription. The amplified RNA molecules are used to
527 prepare scMspJI-seq libraries and sequenced on an Illumina platform.



528

529 **Figure 2 | Cell-to-cell heterogeneity in genome-wide strand-specific methylome**

530 **landscapes in mES cells. (a)** An example of a mES cell (cell #216) that shows similar amounts

531 of 5mCpG on both the plus and the minus strand of each chromosome. **(b)** Another mES cell (cell

532 #526) with asymmetric amounts of 5mCpG between the plus and the minus strand of each

533 chromosome. **(c)** Histogram of Pearson correlations between the 5mCpG levels on the plus and

534 the minus stand over all chromosomes in a cell show that while a majority of cells have similar

535 amounts of 5mCpG on both strands (high Pearson correlation), a small fraction of cells display

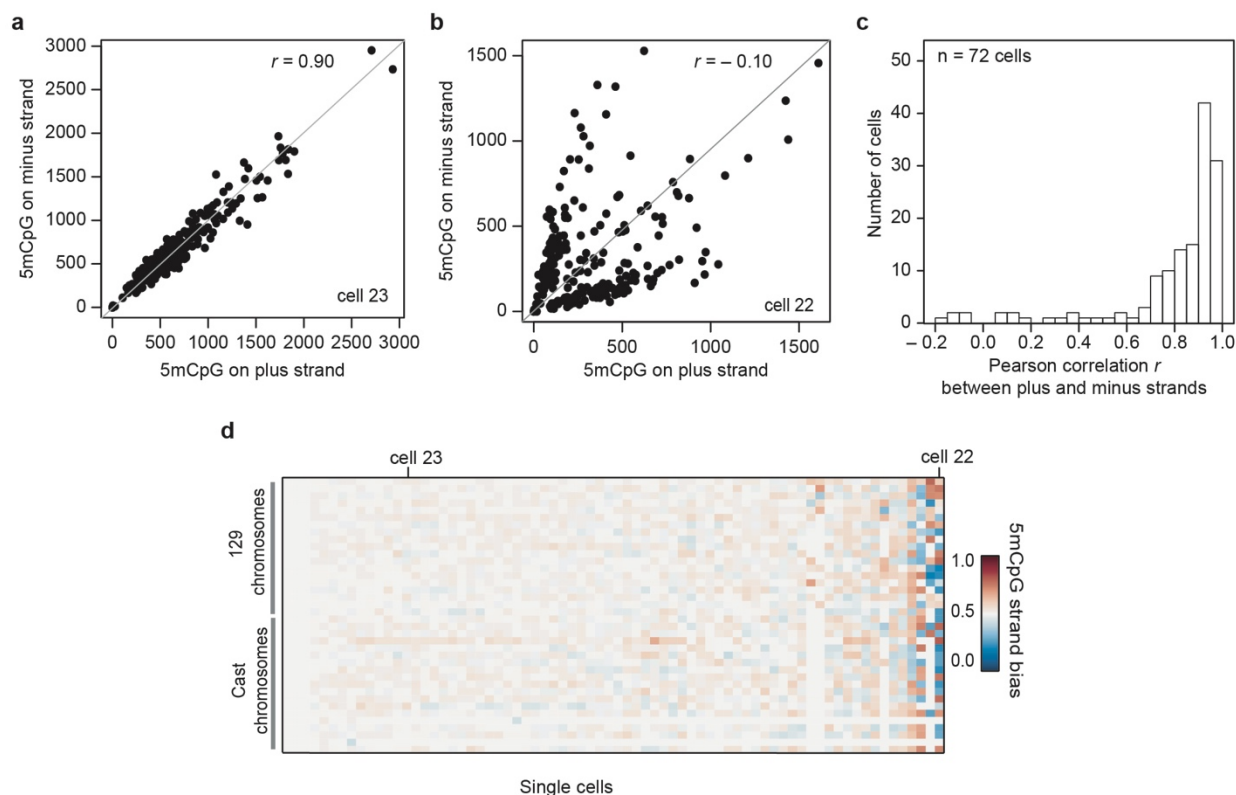
536 unequal levels of 5mCpG between the two strands of each chromosome (low Pearson

537 correlation). **(d)** Ordered heatmap showing 5mCpG strand bias per chromosome for the maternal

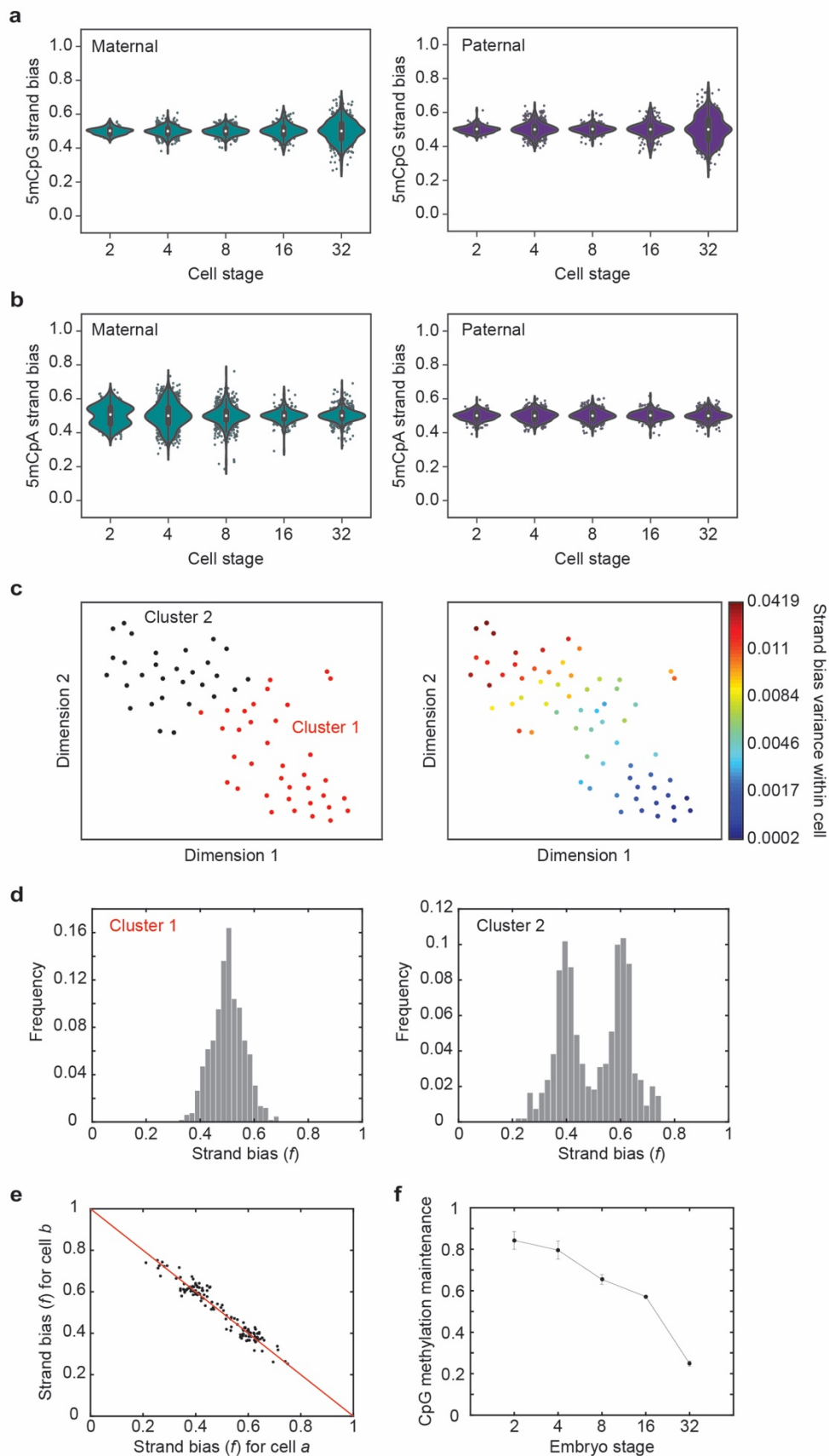
538 and paternal alleles in individual mES cells. **(e)** 5mCpG strand bias of cell #526 (*top*) and cell

539 #216 (*bottom*) for 10 MB bins along the first 9 chromosomes are shown with statistically significant

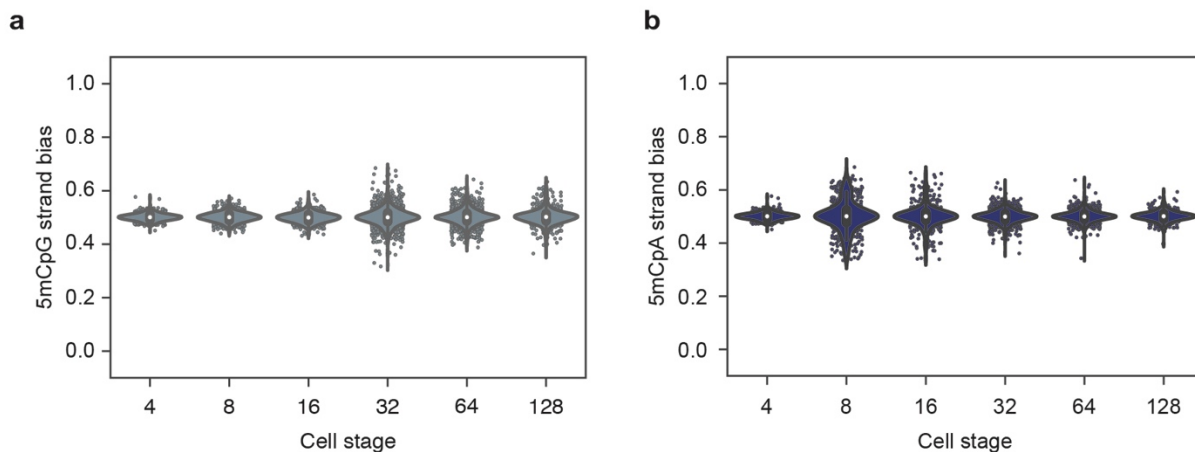
540 ($P < 0.05$, likelihood ratio test) strand biases towards the plus and minus strands shown in red
541 and blue, respectively. Strand biases of bins that are not statistically significant are shown in gray
542 ($P > 0.05$, likelihood ratio test).



543
544 **Figure 3 | Variability in strand-specific 5mCpG profiles in mES cells.** (a) A representative
545 mES cell (cell #23) with similar amounts of 5mCpG within 10 MB bins on both DNA strands. (b)
546 Another representative mES cell (cell #22) with unequal amounts of 5mCpG between the two
547 DNA strands for 10 MB bins. (c) Histogram of Pearson correlations between the 5mCpG levels
548 on the plus and the minus stand over the entire genome (10 MB) in a cell. (d) Ordered heatmap
549 showing 5mCpG strand bias per chromosome for maternal and paternal alleles in individual mES
550 cells ($n=72$). The results in this figure is based on strand-specific reanalysis of single-cell bisulfite
551 sequencing data obtained from previous work by Clark *et al.* ²⁴



553 **Figure 4 | DNA demethylation dynamics in preimplantation mouse embryos.** (a) Violin plots
554 of 5mCpG strand bias for both the maternal (*left*) and paternal (*right*) genome show a tight
555 distribution centered around $f = 0.5$ till the 16-cell stage and a wider distribution at the 32-cell
556 stage of development. (b) For the maternal genome (*left*), 5mCpA strand bias show a bimodal
557 distribution at the 2-cell stage that moves towards a tight unimodal distribution by the 32-cell stage
558 of development. The paternal genome (*right*) shows a unimodal distribution centered at $f = 0.5$
559 throughout preimplantation development till the 32-cell stage. (c) t-SNE map displaying 2 cluster
560 of single cells. These clusters were identified by *k*-means clustering on the 5mCpG strand bias
561 for all paternal chromosomes (*left*). The *right* panel shows the strand bias variance within each
562 cell superimposed on the t-SNE map. (d) The two clusters shown in panel c display dramatically
563 different 5mCpG strand bias distributions – one cluster (*left*) shows a unimodal distribution while
564 the other cluster (*right*) shows a bimodal distribution implying loss of methylation maintenance.
565 (e) Strand bias of chromosomes between anti-correlated cell pairs suggesting that these pairs are
566 sister cells. (f) Bulk hairpin bisulfite sequencing reveals that the fraction of CpG dyads that are
567 symmetrically methylated drops substantially from the 16- to 32-cell stage of development.



568

569 **Figure 5 | DNA demethylation dynamics in preimplantation human embryos.** (a) Violin plots
570 showing 5mCpG strand bias from the 4- to 128-cell stage of human embryogenesis. In the
571 absence of allele specific information, the strand bias represents an average over both alleles.
572 Similar to mouse embryos, human embryos initially show no 5mCpG strand followed by an
573 increase at the 16-cell stage of embryogenesis. (b) Violin plots showing 5mCpA strand bias from
574 the 4- to 128-cell stage of human embryogenesis. 5mCpA strand bias dynamics in human
575 embryos is similar to that observed in mouse embryos in Figure 4b.